VIP Coordination Chemistry Very Important Paper

How to cite: *Angew. Chem. Int. Ed.* **2021**, *60*, 13865–13870
International Edition: doi.org/10.1002/anie.202103267
German Edition: doi.org/10.1002/ange.202103267

Highly Coordinated Heteronuclear Calcium–Iron Carbonyl Cation Complexes $[CaFe(CO)_n]^+$ ($n = 5$–12) with d–d Bonding

Xiaoyang Jin[+], Yuna Bai[+], Yangyu Zhou, Guanjun Wang, Lili Zhao, Mingfei Zhou, and Gernot Frenking**

Abstract: *Heteronuclear calcium–iron carbonyl cation complexes in the form of $[CaFe(CO)_n]^+$ ($n = 5$–12) are produced in the gas phase. Infrared photodissociation spectroscopy in conjunction with quantum chemical calculations confirm that the $n = 10$ complex is the coordination saturated ion where a $Fe(CO)_4$ fragment is bonded with a $Ca(CO)_6$ fragment through two side-on bridging carbonyl ligands. Bonding analysis indicates that it is best described by the bonding interactions between a $[Ca(CO)_6]^{2+}$ dication and an $[Fe(CO)_4]^-$ anion forming a Fe→Ca d–d dative bond in the $[(CO)_6Ca–Fe(CO)_4]^+$ structure, which enriches the pool of experimentally observed complexes of calcium that mimic transition metal compounds. The molecule is the first example of a heteronuclear carbonyl complex featuring a d–d bond between calcium and a transition metal.*

The alkaline earth elements are among the most electropositive elements in the periodic table and they are usually classified as main-group elements that belong to the s-block atoms. They readily lose the outermost valence s electrons to form ionic compounds. The coordination chemistry of alkaline earth metal ions was thus considered to be relatively simple and uninteresting for quite a long time. The metal–ligand interactions are expected to be predominantly electrostatic with negligible orbital interactions, and are mostly governed by Coulomb interactions and steric factors.[1,2] However, recent investigations indicate that the alkaline earth elements have a much richer coordination chemistry than hitherto thought. Many alkaline earth metal coordination compounds show unusual geometric and electronic structures with covalent bonding character.[3–7] In particular, the zero and monovalent heavier alkaline earth metals show an unexpected bonding situation that mimic transition metals.[8-11] It was found that the heavier group-2 atoms form octa-coordinated carbonyl and dinitrogen complexes $M(CO)_8$ and $M(N_2)_8$ (M = Ca, Sr, Ba) as well as tribenzene complexes $M(Bz)_3$ (M = Sr, Ba) in solid neon matrix.[9–11] The bonding situation in these complexes is similar to transition metal complexes following the 18 electron rule with the metal d orbitals playing a crucial role in metal–ligand bonding. The octa-coordinated carbonyl and dinitrogen complexes of monovalent metal ions were also formed in the gas phase, which show similar bonding as the neutral complexes.[9,10] Computational investigations indicate that d orbitals also contribute significantly to the bonding of divalent heavier alkaline earth metal complexes.[12] A recent theoretical analysis of the chemical bonds in alkaline earth oxides, imides and dihydrides as well as a calcium complex suggests that the valence orbitals of Ca, Sr, Ba comprise the (n)s and (n−1)d AOs, the latter being much more important than the former, which is a characteristic feature of the transition metals.[13]

Here we report the generation and spectroscopic characterization of heteronuclear calcium–iron carbonyl cation complexes in the gas phase. Infrared spectroscopy in conjunction with theoretical calculations confirm that the coordinatively saturated $[CaFe(CO)_{10}]^+$ cation possesses a $[Ca(CO)_6]^{2+}[Fe(CO)_4]^-$ structure involving significant Fe–Ca d–d dative bonding supported by two side-on bridging carbonyl ligands.

The heteronuclear calcium–iron carbonyl cation complexes are prepared by a pulsed laser vaporization/supersonic expansion ion source in the gas phase, and are detected by mass-selected infrared photodissociation spectroscopy in the carbonyl stretching vibrational frequency region as described in detail previously.[14] The mass spectrum of ion complexes produced by pulsed laser vaporization of a pure calcium metal target in an expansion of helium seeded with carbon monoxide with traces of $Fe(CO)_5$ impurity is shown in Figure 1. The spectrum is dominated by a progression of mass peaks that can be assigned to the heteronuclear calcium–iron carbonyl cation complexes in the form of $[CaFe(CO)_n]^+$ ($n = 4$–12). The $[Ca(CO)_n]^+$ ($n = 0$–5) peaks are also presented. The $[CaFe(CO)_{10}]^+$ cation is always the most intense peak among this series of cations at different experimental

[*] X. Jin,[+] Y. Zhou, G. Wang, M. Zhou
Department of Chemistry, Shanghai Key Laboratory of Molecular Catalysts and Innovative Materials, Fudan University
Shanghai 200438 (China)
E-mail: mfzhou@fudan.edu.cn
Y. Bai,[+] L. Zhao, G. Frenking
Institute of Advanced Synthesis, School of Chemistry and Molecular Engineering, Nanjing Tech University
Nanjing 211816 (China)
G. Frenking
Fachbereich Chemie, Philipps-Universität Marburg
Hans-Meerwein-Strasse 4, 35043 Marburg (Germany)
E-mail: frenking@chemie.uni-marburg.de
[+] These authors contributed equally to this work.
Supporting information and the ORCID identification number(s) for the author(s) of this article can be found under: https://doi.org/10.1002/anie.202103267.

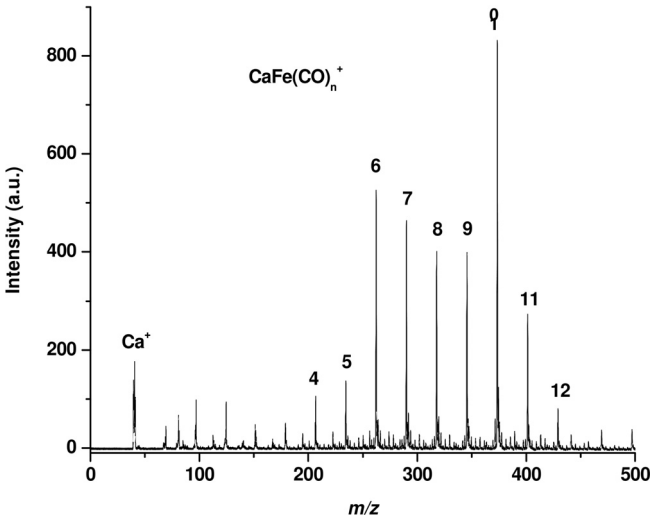

Figure 1. Mass spectrum of heteronuclear calcium–iron carbonyl cation complexes produced by pulsed laser vaporization of a calcium metal target in an expansion of helium seeded by carbon monoxide with traces of $Fe(CO)_5$ impurity.

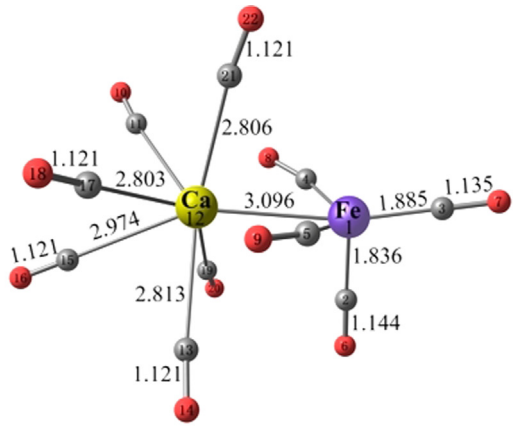

Bond	12-4	2.680	12-5	2.680
	12-11	2.803	11-10	1.121
	12-19	2.813	19-20	1.121
	1-5	1.765	5-9	1.179
	1-4	1.765	4-8	1.179
Angle	∠1-12-17	125.2	∠12-1-2	93.9
	∠1-12-15	153.0	∠12-1-3	167.7
	∠1-12-13	88.4	∠12-1-5	59.7
	∠1-12-21	78.7	∠5-1-2	101.4
	∠5-1-3	117.3	∠15-12-21	128.3
	∠1-3-7	179.8	∠12-15-16	179.5
	∠12-13-14	174.2	∠12-17-18	173.1
	∠12-19-20	174.2	∠12-11-10	173.1
	∠12-21-22	173.4	∠1-2-6	179.1
	∠1-12-5	34.6	∠1-5-9	163.1
	∠1-12-4	34.6	∠1-4-8	163.1

Figure 2. Calculated equilibrium geometry of the $[CaFe(CO)_{10}]^+$ cation at the B3LYP/6–311 + G(d) level. Bond lengths are given in Å, angles in degree. The color code is: gray (C); yellow (Ca); purple (Fe); red (O).

conditions, suggesting that this cation is the coordination saturated complex. The higher coordinated complexes involve weakly bound ligands attached to the external surface of the stable $[CaFe(CO)_{10}]^+$ cation, which are formed only because of the cold supersonic beam conditions.

The $n = 9$–11 cation complexes are each mass-selected for infrared photodissociation. All these cation complexes dissociate by losing CO ligand(s) with unfocused IR laser. The vibrational spectra in the CO stretching frequency region for the $n = 9$–11 complexes are shown in Figure S1 of Supporting Information. The spectra for the $n = 9$ and 10 complexes are quite similar, each exhibits five well-resolved bands in the carbonyl stretching frequency region. Similar bands are also presented in the spectrum of the $n = 11$ complex. In addition, a weak band at 2157 cm^{-1} is also observed for the $n = 11$ complex. This band is slightly blue-shifted from that of free CO and is due to the absorption of a weakly bound CO ligand.[15] The observation of a weakly bound CO ligand confirms that the $n = 11$ cation is a weakly bound complex involving a $[CaFe(CO)_{10}]^+$ core cation. The observation of two bands below 1800 cm^{-1} implies that the cation involves two bridged carbonyl ligands.[16] The other bands are due to vibrations of the terminally bonded carbonyl ligands. The band in the 2200 cm^{-1} region, which is about 60 cm^{-1} blue-shifted from that of free CO, is due to vibration(s) of carbonyl ligand(s) that is coordinated to a highly electrophilic metal center with negligible metal-to-CO backdonation.[17] The spectral feature suggests that the $[CaFe(CO)_{10}]^+$ cation is coordinatively saturated at calcium and iron.

We optimized the geometry of $[CaFe(CO)_{10}]^+$ using density functional theory (DFT) at the B3LYP/6–311 + G(d) level of theory. Details of the calculations are given in Supporting Information. Figure 2 shows the calculated geometry and the most important bond lengths and angles. The optimized structure of $[CaFe(CO)_{10}]^+$ has C_s symmetry and a $^2A'$ electronic state featuring a $Fe(CO)_4$ fragment that is bonded to a $Ca(CO)_6$ moiety with a Ca–Fe distance of 3.096 Å and two side-on bridging carbonyl ligands of $Fe(CO)_4$ tilted toward Ca with a bending angle Ca-Fe-CO of 59.7°. The calculated Ca–Fe distance of 3.096 Å is slightly longer than the sum of standard single bond radii of Ca and Fe, which is 2.87 Å.[18] Calculations using a different (BP86) functional give a very similar geometry with a somewhat shorter Ca–Fe distance of 2.955 Å (Figure S2). We have chosen B3LYP for this project, because it gives the best agreement of the calculated IR spectrum with the observed data (see below). The calculated geometry indicates that the $Fe(CO)_4$ and $Ca(CO)_6$ moieties are mainly bonded by direct Fe–Ca interactions and by two bridging CO ligands. Please note that one of the CO ligands of the $Ca(CO)_6$ moiety, which is in a *trans* position to the $Fe(CO)_4$ fragment, has a much wider bond angle of 153.0° and it has a significantly longer Ca–CO bond of 2.974 Å than the other Ca–CO bonds, which are between 2.803–2.813 Å.

Table 1 shows the comparison of the experimental and calculated C-O stretching modes. The full set of calculated vibrational frequencies and IR intensities is given in Table S3 of Supporting Information. The agreement between the

Table 1: Comparison between experimental and calculated (B3LYP/6–311 + G(d) level) vibrational frequencies (cm^{-1}) of $[CaFe(CO)_{10}]^+$.

Exptl.	Calcd.[b]	Mode
2195	2191–2202[a]	CO str. of $Ca(CO)_6$
2107	2078	sym. str. of terminal COs of $Fe(CO)_4$
2004	2011	asym. str. of terminal COs of $Fe(CO)_4$
1796	1812	sym. str. of bridged COs of $Fe(CO)_4$
1743	1766	asym. str. of bridged COs of $Fe(CO)_4$

[a] Six narrow-spaced lines. [b] The calculated frequencies are scaled by a factor of 0.969 which is given by the ratio of the experimental (2143 cm^{-1}) and calculated (2212 cm^{-1}) stretching frequency of free CO.

measured and the theoretical frequencies of the CO stretching mode is very good. This comes to the fore when the simulated IR spectrum shown in Figure 3b is compared to the experimental spectrum in Figure 3a. There is no doubt that the observed cation $[CaFe(CO)_n]^+$ exhibits the $[(CO)_6Ca–Fe(CO)_4]^+$ structure shown in Figure 2.

Figure 4a shows the Laplacian distribution of the charge density $\nabla^2\rho(\mathbf{r})$ of $[CaFe(CO)_{10}]^+$ in the plane Ca-Fe-CO where the CO is a bridging carbonyl. There is a bond critical point (bcp) and bond path for the Ca–Fe and Fe–CO interactions but not for the Ca–CO pair. It has been shown before that the absence of a bcp and a bond path between two atoms does not rule out strong attractive interactions.[19] The curvature of the charge distribution does not yield a critical point between Ca and the carbon atom of the tilted CO but the bending angle suggests some attraction between the atoms. Figure 4a shows also the atomic partial charges given by the QTAIM analysis. The metal atoms both carry positive charges of 0.59 e (Fe) and 1.59 e (Ca) whereas the oxygen atoms have uniformly large negative charges between −1.04 e and −1.17 e. Significant differences are found between the positively charged carbon atoms of the CO ligands bonded to Fe, which are between 0.66 e and 0.95 e, and the C atoms of the CO ligands bonded to Ca, which are between 1.06 e and 1.08 e. The calculated charge distribution suggests that the $Ca(CO)_6$ fragment carries a positive charge of 1.73 e whereas the $Fe(CO)_4$ fragment has a negative charge of −0.73 e. The unpaired electron of the radical cation is nearly exclusively localized at the Fe atom where it occupies mainly a 3d(π) AO. Figure 4b shows the calculated spin density of $[CaFe(CO)_{10}]^+$.

More detailed information about the bonding situation in $[CaFe(CO)_{10}]^+$ is provided by the EDA–NOCV analysis of the cation. We used the fragments $[Ca(CO)_6]^q$ and $[Fe(CO)_4]^q$

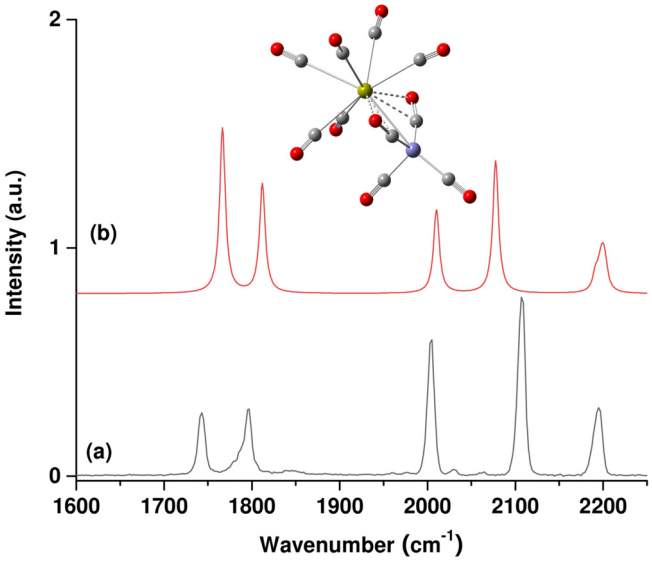

Figure 3. a) Experimental and b) simulated IR spectra of $[CaFe(CO)_{10}]^+$. The simulated spectrum is obtained from the scaled (0.969) harmonic vibrational frequencies and intensities calculated at the B3LYP/6–311 + G(d) level by applying Lorentzian line shape function with 5 cm^{-1} full-width-at-half-maximum.

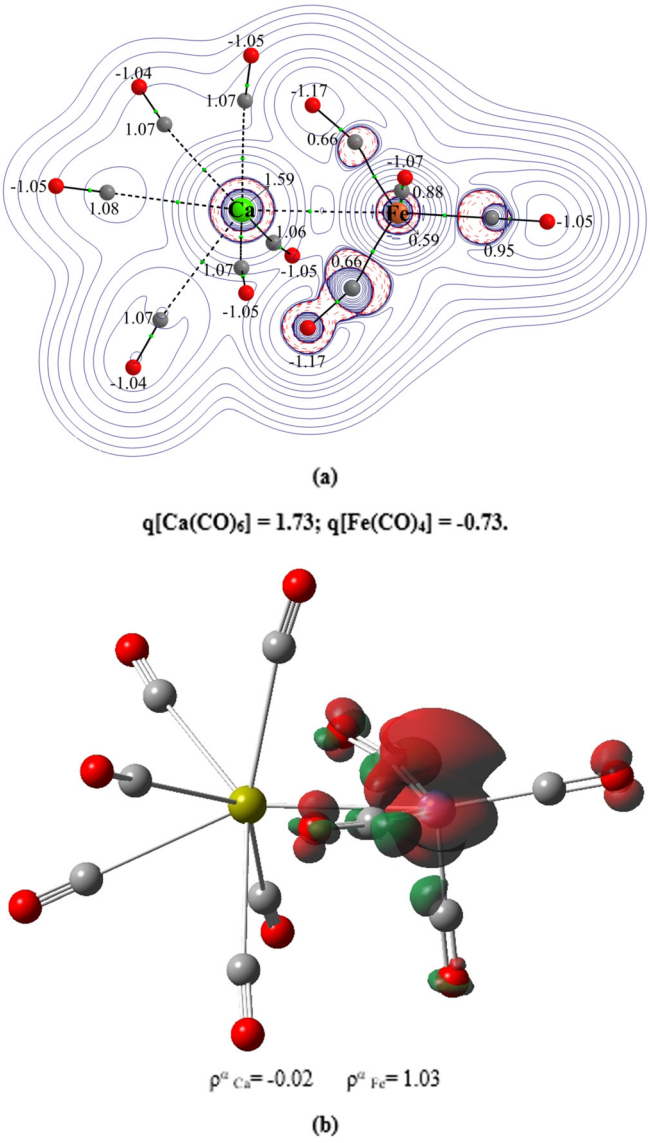

Figure 4. a) Partial charges q and Laplacian distribution of the charge density $\nabla^2\rho(\mathbf{r})$ of $[CaFe(CO)_{10}]^+$ in the plane Ca-C4-Fe. Red lines indicate areas of charge concentration ($\nabla^2\rho(\mathbf{r}) < 0$) while blue lines show areas of charge depletion ($\nabla^2\rho(\mathbf{r}) > 0$) at the B3LYP/6–311 + G(d) level. The solid lines connecting the atomic nuclei are the bond paths. Green dots are bond critical points, and red dots are ring critical points. b) Calculated spin density of $[CaFe(CO)_{10}]^+$ in the doublet state at the B3LYP/6–311 + G(d) level. The calculated spin densities are taken from the Mulliken atomic spin densities (in a.u.).

with different charges q and electronic states as interacting species. The best description of the interatomic interactions in the complex is given by using the dication $[Ca(CO)_6]^{2+}$ and the radical anion $[Fe(CO)_4]^-$ as interacting fragments, because they give the smallest value for the orbital interaction ΔE_{orb}.[20] Table 2 gives the numerical results of the EDA–NOCV calculations along with the results using the fragments $[Ca(CO)_6]^+$ and neutral $Fe(CO)_4$ as interacting species, which are the products of the Ca–Fe bond breakage. The latter results consider all interactions during bond formation, while the use of the former fragments describe the bond finally formed. The EDA–NOCV method is capable of addressing both situations.

Table 2: EDA–NOCV results of $[CaFe(CO)_{10}]^+$ by using the double(D) and singlet(S) fragments at the B3LYP/TZ2P//B3LYP/ 6-311+G(d) level. Energy values are given in kcal mol^{-1}.

Fragments	$[Ca(CO)_6]^+$ (D) + $Fe(CO)_4$(S)	$[Ca(CO)_6]^{2+}$ (S) + $[Fe(CO)_4]^-$ (D)
ΔE_{int}	−63.2	−209.9
ΔE_{Pauli}	66.4	45.6
ΔE_{elstat}[a]	−34.7 (26.8%)	−186.4 (73.0%)
ΔE_{orb}[a]	−94.8 (73.2%)	−69.1 (27.0%)
ΔE_{orb1}[b]	−62.5(65.9%)	−20.6 (29.8%)
ΔE_{orb2}[b]	−13.8 (14.6%)	−8.0 (11.6%)
ΔE_{orb3}[b]	−4.2 (4.4%)	−7.3 (10.6%)
ΔE_{orb4}[b]	–	−5.8 (8.4%)
ΔE_{orb5}[b]	–	−5.4 (7.8%)
$\Delta E_{orb(rest)}$	−14.3 (15.1%)	−22.0 (31.8%)

[a] The values in parentheses give the percentage contribution to the total attractive interactions $\Delta E_{elstat} + \Delta E_{orb}$. [b] The values in parentheses give the percentage contribution to the total orbital interactions ΔE_{orb}.

The data in Table 2 show that the major contribution to the attractive interactions during bond formation between $[Ca(CO)_6]^+$ and $Fe(CO)_4$ comes from the orbital (covalent) term ΔE_{orb}, which provides 73% to the attractive forces whereas the electrostatic (Coulomb) interaction ΔE_{elstat} constitutes 27%. This is reasonable, because the driving force for the formation of covalent bonding is due to the interference of the wavefunctions.[21] The ratio reverses when the polar bond is finally formed, where the Coulomb attraction accounts for 73% of the attractive forces.

The breakdown of the orbital term ΔE_{orb} into pairwise orbital interactions shows that the strongest individual contribution in the complex comes from the donation of the HOMO of $[Fe(CO)_4]^-$ to low-lying vacant MOs of $[Ca(CO)_6]^{2+}$ which amounts to $\Delta E_{orb1} = -20.6$ kcal mol^{-1}. This becomes viable by inspecting the associated deformation density $\Delta\rho_1$ and the connected fragment orbitals, which are shown in Figure 5a. The shape of $\Delta\rho_1$ indicates that the charge flow occupies not only the Ca–Fe bonding region but also the bridging CO groups. The second strongest orbital interaction $\Delta E_{orb2} = -8.0$ kcal mol^{-1} comes from the donation of the singly occupied π MO of $[Fe(CO)_4]^-$ to the LUMO + 3 of $[Ca(CO)_6]^{2+}$ building a singly occupied Ca–Fe π orbital (Figure 5b). The next three contributions $\Delta E_{orb3} - \Delta E_{orb5}$ come from orbital interactions which are due to the covalent attraction between the bridging CO ligands of the $[Fe(CO)_4]^-$ fragment to Ca (Figures 5c–e). Note that several acceptor orbitals of the $[Ca(CO)_6]^{2+}$ fragment are antibonding with regard to the Ca–CO(trans) bond, which explains the very long bond. Further examination of the acceptor orbitals at $[Ca(CO)_6]^{2+}$ reveals a large participation of the 3d AO of Ca. Thus, the overall orbital interactions between $[Ca(CO)_6]^{2+}$ and $[Fe(CO)_4]^-$ are the combination of Ca–Fe bond formation accompanied by the attraction between Ca and the bridging CO ligands that uses the 3d AOs of calcium as acceptor orbitals. This is a striking example for the strength of the EDA–NOCV method, which gives very detailed information about the individual orbital interactions between the chose fragments. The remaining orbital term $\Delta E_{orb(rest)}$ comes mainly from intra-fragment charge polarization of the charged fragments. The positive charge of the cation enhances the preference of the 3d AOs of Ca for covalent bonding. This is because the first excited state of Ca^+ is ^2D ($4s^03d^1$), which is only 30 kcal mol^{-1} above the ^2S state whereas the ^3D ($4s^13d^1$) state is the second excited state of neutral Ca following ^3P ($4s^14p^1$) and which is 57.1 kcal mol^{-1} higher than the ^1S ($4s^2$) ground state.[22]

It is interesting to compare the Nalewajski–Mrozek bond order[23] P(A–B) of the Ca–Fe bond in $[(CO)_6Ca–Fe(CO)_4]^+$ with the Ca–CO values. The calculated value P(Ca–Fe) = 0.11 indicates a weak single bond, which is, however, larger than the P(Ca–CO) values, which range from 0.05 to 0.08. The complete list of the Nalewajski–Mrozek bond orders is given in Table S4 of Supporting Information.

In summary, we report the observation of the heteronuclear calcium–iron carbonyl cation complexes $[CaFe(CO)_n]^+$ (n = 5–12) in the gas phase. Infrared photodissociation spectroscopy in conjunction with quantum chemical calculations confirm that the $n = 10$ complex is the coordination saturated ion where a $Fe(CO)_4$ fragment is bonded with a $Ca(CO)_6$ moiety through two side-on bridging carbonyl ligands. Bonding analysis indicates that the complex is best described by the bonding interactions between a $[Ca(CO)_6]^{2+}$ dication and an $[Fe(CO)_4]^-$ anion forming a Fe–Ca d–d dative bond that is completed by the attraction between Ca and the bridging CO ligands. The observation of $[(CO)_6Ca–Fe(CO)_4]^+$ enriches the pool of experimentally observed complexes of calcium that mimic transition metal compounds. The molecule is the first example of a heteronuclear carbonyl complex featuring a d–d bond between calcium and a transition metal.

Acknowledgement

The experimental work was financially supported by the National Natural Science Foundation of China (grant number 21688102). L.Z. and G.F. acknowledge financial support from Nanjing Tech University (grant numbers 39837123, 39837132) and SICAM Fellowship from Jiangsu National Synergetic Innovation Center for Advanced Materials, Natural Science Foundation of Jiangsu Province for Youth (grant number BK20170964), National Natural Science Foundation of China

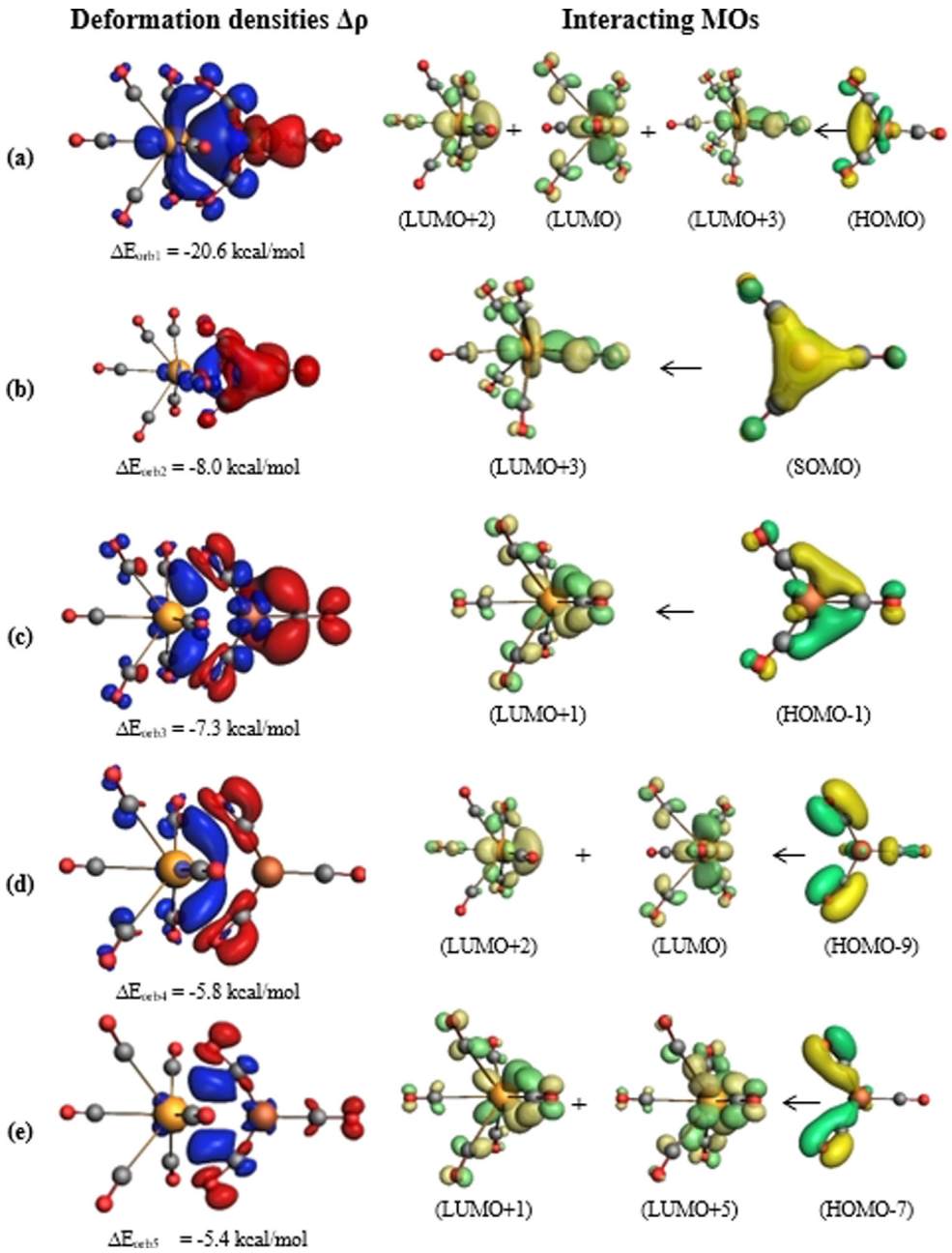

Figure 5. Plot of the deformation densities $\Delta\rho$ of the five most important pairwise orbital interactions (See Table 2) and shape of the most relevant associated MOs of the fragments $[Ca(CO)_6]^{2+}$ (S) and $[Fe(CO)_4]^{-}$ (D) fragments in $[CaFe(CO)_{10}]^{+}$. The direction of the charge flow is red→blue.

(grant number 21703099). G.F. is grateful to the Deutsche Forschungsgemeinschaft for financial support. Open access funding enabled and organized by Projekt DEAL.

Conflict of interest

The authors declare no conflict of interest.

Keywords: bonding analysis · heteronuclear complexes · infrared spectroscopy · matrix isolation · quantum chemical calculations

[1] a) N. S. Poonia, A. V. Bajaj, *Chem. Rev.* **1979**, *79*, 389–445; b) A. V. Bajaj, N. S. Poonia, *Coord. Chem. Rev.* **1988**, *87*, 55–213; c) P. G. Daniele, C. Foti, A. Gianguzza, E. Prenesti, S. Sammartano, *Coord. Chem. Rev.* **2008**, *252*, 1093–1107.

[2] a) P. J. Chirik, *Organometallics* **2019**, *38*, 195–197; b) S. C. Roşca, E. Caytan, V. Dorcet, T. Roisnel, J. F. Carpentier, Y. Sarazin, *Organometallics* **2017**, *36*, 1269–1277; c) A. Torvisco, K. Ruhlandt-Senge, *Inorg. Chem.* **2011**, *50*, 12223–12240; d) W. D. Buchanan, D. G. Allis, K. Ruhlandt-Senge, *Chem. Commun.* **2010**, *46*, 4449–4465.

[3] a) S. A. Couchman, N. Holzmann, G. Frenking, D. J. D. Wilson, J. L. Dutton, *Dalton Trans.* **2013**, *42*, 11375–11384; b) K. J. Iversen, S. A. Couchman, D. J. D. Wilson, J. L. Dutton, *Coord.*

Chem. Rev. **2015**, *297 – 298*, 40 – 48; c) L. C. Perera, O. Raymond, W. Henderson, P. J. Brothers, P. G. Plieger, *Coord. Chem. Rev.* **2017**, *352*, 264 – 290.

[4] a) G. J. Wang, Y. Y. Zhou, X. Y. Jin, J. Y. Jin, M. F. Zhou, *Angew. Chem. Int. Ed.* **2021**, *60*, 1651 – 1655; *Angew. Chem.* **2021**, *133*, 1675 – 1679; b) G. H. Deng, S. Pan, G. J. Wang, L. L. Zhao, M. F. Zhou, G. Frenking, *Angew. Chem. Int. Ed.* **2020**, *59*, 10603 – 10609; *Angew. Chem.* **2020**, *132*, 10690 – 10696; c) G. H. Deng, S. Pan, G. J. Wang, L. L. Zhao, M. F. Zhou, G. Frenking, *Angew. Chem. Int. Ed.* **2020**, *59*, 18201 – 18207; *Angew. Chem.* **2020**, *132*, 18358 – 18364; d) M. Arrowsmith, H. Braunschweig, M. A. Celik, T. Dellermann, R. D. Dewhurst, W. C. Ewing, K. Hammond, T. Kramer, I. Krummenacher, J. Mies, K. Radacki, J. K. Schuster, *Nat. Chem.* **2016**, *8*, 890 – 894.

[5] a) S. P. Green, C. Jones, A. Stasch, *Science* **2007**, *318*, 1754 – 1757; b) C. Jones, *Nat. Rev. Chem.* **2017**, *1*, 0059; c) A. J. Boutland, D. Dange, A. Stasch, L. Maron, C. Jones, *Angew. Chem. Int. Ed.* **2016**, *55*, 9239 – 9243; *Angew. Chem.* **2016**, *128*, 9385 – 9389.

[6] a) V. Nesterov, D. Reiter, P. Bag, P. Frisch, R. Holzner, A. Porzelt, S. Inoue, *Chem. Rev.* **2018**, *118*, 9678 – 9842; b) K. M. Fromm, *Coord. Chem. Rev.* **2020**, *408*, 213193.

[7] a) A. S. S. Wilson, M. S. Hill, M. F. Mahon, C. Dinoi, L. Maron, *Science* **2017**, *358*, 1168 – 1171; b) H. Bauer, M. Alonso, C. Fischer, B. Rçsch, H. Elsen, S. Harder, *Angew. Chem. Int. Ed.* **2018**, *57*, 15177 – 15182; *Angew. Chem.* **2018**, *130*, 15397 – 15402; c) H. Bauer, M. Alonso, C. Farber, H. Elsen, J. Pahl, A. Causero, G. Ballmann, F. De Proft, S. J. Harder, *Nat. Catal.* **2018**, *1*, 40 – 47.

[8] X. Wu, L. L. Zhao, D. D. Jiang, I. Fernandez, R. Berger, M. F. Zhou, G. Frenking, *Angew. Chem. Int. Ed.* **2018**, *57*, 3974 – 3980; *Angew. Chem.* **2018**, *130*, 4038 – 4044.

[9] a) X. Wu, L. L. Zhao, J. Y. Jin, S. Pan, W. Li, X. Y. Jin, G. J. Wang, M. F. Zhou, G. Frenking, *Science* **2018**, *361*, 912 – 916; b) P. B. Armentrout, *Science* **2018**, *361*, 849 – 850; c) X. M. Yang, *Nat. Sci. Rev.* **2019**, *6*, 8 – 9.

[10] Q. Wang, S. Pan, S. J. Lei, J. Y. Jin, G. H. Deng, G. J. Wang, L. L. Zhao, M. F. Zhou, G. Frenking, *Nat. Commun.* **2019**, *10*, 3375.

[11] Q. Wang, S. Pan, Y. B. Wu, G. H. Deng, J. H. Bian, G. J. Wang, L. L. Zhao, M. F. Zhou, G. Frenking, *Angew. Chem. Int. Ed.* **2019**, *58*, 17365 – 17374; *Angew. Chem.* **2019**, *131*, 17526 – 17535.

[12] a) L. Garcia, M. D. Anker, M. F. Mahon, L. Maron, M. S. Hill, *Dalton Trans.* **2018**, *47*, 12684 – 12693; b) D. Schuhknecht, T. P. Spaniol, I. Douair, L. Maron, J. Okuda, *Chem. Commun.* **2019**, *55*, 14837 – 14839; c) T. Bettens, S. Pan, F. De Proft, G. Frenking, P. Geerlings, *Chem. Eur. J.* **2020**, *26*, 12785 – 12793.

[13] I. Fernandez, N. Holzmann, G. Frenking, *Chem. Eur. J.* **2020**, *26*, 14194 – 14210.

[14] a) G. J. Wang, C. X. Chi, X. P. Xing, C. F. Ding, M. F. Zhou, *Sci. China Chem.* **2014**, *57*, 172 – 177; b) G. J. Wang, C. X. Chi, J. M. Cui, X. P. Xing, M. F. Zhou, *J. Phys. Chem. A* **2012**, *116*, 2484 – 2489.

[15] a) A. M. Ricks, Z. E. Reed, M. A. Duncan, *J. Mol. Spectrosc.* **2011**, *266*, 63 – 74; b) G. J. Wang, M. F. Zhou, *Chin. J. Chem. Phys.* **2018**, *31*, 1 – 11.

[16] a) C. X. Chi, H. Qu, L. Y. Meng, F. C. Kong, M. B. Luo, M. F. Zhou, *Angew. Chem. Int. Ed.* **2017**, *56*, 14096 – 14101; *Angew. Chem.* **2017**, *129*, 14284 – 14289; b) P. S. Braterman, *Metal Carbonyl Spectra*, Academic Press, London, **1975**; c) M. F. Zhou, L. Andrews, C. W. Bauschlicher, Jr., *Chem. Rev.* **2001**, *101*, 1931 – 1961.

[17] a) A. J. Lupinetti, G. Frenking, S. H. Strauss, *Angew. Chem. Int. Ed.* **1998**, *37*, 2113 – 2116; *Angew. Chem.* **1998**, *110*, 2229 – 2232; b) A. J. Lupinetti, S. Fau, G. Frenking, S. H. Strauss, *J. Phys. Chem. A* **1997**, *101*, 9551 – 9559; c) A. J. Lupinetti, V. Jonas, W. Thiel, S. H. Strauss, G. Frenking, *Chem. Eur. J.* **1999**, *5*, 2573 – 2583; d) A. Diefenbach, F. M. Bickelhaupt, G. Frenking, *J. Am. Chem. Soc.* **2000**, *122*, 6449 – 6458; e) M. H. Chen, Q. N. Zhang, M. F. Zhou, D. M. Andrada, G. Frenking, *Angew. Chem. Int. Ed.* **2015**, *54*, 124 – 128; *Angew. Chem.* **2015**, *127*, 126 – 130.

[18] P. Pyykkö, M. Atsumi, *Chem. Eur. J.* **2009**, *15*, 186 – 197.

[19] Examples: a) M. Mousavi, G. Frenking, *Organometallics* **2013**, *32*, 1743 – 1751; b) M. Mousavi, G. Frenking, *J. Organomet. Chem.* **2013**, *748*, 2 – 7.

[20] Recent examples: a) Q. N. Zhang, W.-L. Li, C. Q. Xu, M. H. Chen, M. F. Zhou, J. Li, D. M. Andrada, G. Frenking, *Angew. Chem. Int. Ed.* **2015**, *54*, 11078 – 11083; *Angew. Chem.* **2015**, *127*, 11230 – 11235; b) D. M. Andrada, G. Frenking, *Angew. Chem. Int. Ed.* **2015**, *54*, 12319 – 12324; *Angew. Chem.* **2015**, *127*, 12494 – 12500; c) C. Mohapatra, S. Kundu, A. N. Paesch, R. Herbst-Irmer, D. Stalke, D. M. Andrada, G. Frenking, H. W. Roesky, *J. Am. Chem. Soc.* **2016**, *138*, 10429 – 10432; d) L. T. Scharf, M. Andrada, G. Frenking, V. H. Gessner, *Chem. Eur. J.* **2017**, *23*, 4422 – 4434; e) M. Hermann, G. Frenking, *Chem. Eur. J.* **2017**, *23*, 3347 – 3356; f) D. C. Georgiou, L. Zhao, D. J. D. Wilson, G. Frenking, J. L. Dutton, *Chem. Eur. J.* **2017**, *23*, 2926 – 2934; g) D. M. Andrada, J. L. Casalz-Sainz, A. M. Pendas, G. Frenking, *Chem. Eur. J.* **2018**, *24*, 9083 – 9089; h) P. Jerabek, P. Schwerdtfeger, G. Frenking, *J. Comput. Chem.* **2019**, *40*, 247 – 264; i) R. Saha, S. Pan, G. Merino, P. K. Chattaraj, *Angew. Chem. Int. Ed.* **2019**, *58*, 8372 – 8377; *Angew. Chem.* **2019**, *131*, 8460 – 8465.

[21] L. Zhao, W. H. E. Schwarz, G. Frenking, *Nat. Rev. Chem.* **2019**, *3*, 35 – 47.

[22] C. E. Moore, Atomic Energy Levels (Natl. Bur. Stand. U.S. Circ. No. 467, U.S. GPO Washington, D.C., **1958**.

[23] a) R. F. Nalewajski, J. Mrozek, *Int. J. Quantum Chem.* **1994**, *51*, 187 – 200; b) R. F. Nalewajski, J. Mrozek, S. J. Formosinho, A. J. C. Varandas, *Int. J. Quantum Chem.* **1994**, *52*, 1153 – 1176; c) R. F. Nalewajski, J. Mrozek, *Int. J. Quantum Chem.* **1996**, *57*, 377 – 389.

Manuscript received: March 5, 2021
Revised manuscript received: April 1, 2021
Accepted manuscript online: April 7, 2021
Version of record online: May 10, 2021

